Enhanced Superconducting Diode Effect due to Coexisting Phases

Sayan Banerjee and Mathias S. Scheurer
Institute for Theoretical Physics III, University of Stuttgart, 70550 Stuttgart, Germany
and Institute for Theoretical Physics, University of Innsbruck, Innsbruck A-6020, Austria

(Received 14 April 2023; accepted 14 December 2023; published 22 January 2024)

The superconducting diode effect refers to an asymmetry in the critical supercurrent $J_c(\hat{n})$ along opposite directions, $J_c(\hat{n}) \neq J_c(-\hat{n})$. While the basic symmetry requirements for this effect are known, it is, for junction-free systems, difficult to capture within current theoretical models the large current asymmetries $J_c(\hat{n})/J_c(-\hat{n})$ recently observed in experiment. We here propose and develop a theory for an enhancement mechanism of the diode effect arising from spontaneous symmetry breaking. We show—both within a phenomenological and a microscopic theory—that there is a coupling of the supercurrent and the underlying symmetry-breaking order parameter. This coupling can enhance the current asymmetry significantly. Our work might not only provide a possible explanation for recent experiments on trilayer graphene but also pave the way for future realizations of the superconducting diode effect with large current asymmetries.

DOI: 10.1103/PhysRevLett.132.046003

Diodes, which are characterized by a highly asymmetric relation between resistance R and current $\boldsymbol{J}$, $R(\boldsymbol{J}) \neq R(-\boldsymbol{J})$, are an integral part of modern-day electronics. A superconductor where the critical current J_c is different along opposite directions, $J_c(\hat{n}) > J_c(-\hat{n})$, can realize a superconducting analog of a diode in the sense that $R(-J\hat{n}) \neq R(J\hat{n}) = 0$, if $J_c(-\hat{n}) < J < J_c(\hat{n})$. While asymmetries in superconducting current-voltage relations in low-symmetry superconductors had been observed before (see, e.g., [1–3]), the potential technological applications of and fundamental scientific questions associated with this superconducting diode effect (SDE) have attracted significant experimental [4–28] and theoretical [29–59] attention in recent years; this led to a variety of different realizations both in tunnel-junction setups [10–24] and in single junction-free superconducting phases [4–9,25–28]. Importantly, critical current asymmetries in superconductors require broken time-reversal symmetry (TRS), which can not only be achieved by applying a magnetic field [4–17], a current [21,22], or magnetic proximity [23,24,27,28], but also result from *spontaneous* TRS breaking in a junction [18–20] or homogeneous superconductor [25,26]; aside from the fundamental interest in the competition of magnetism and superconductivity in a single electron liquid, this might also be useful for integrated designs where external fields are not practical. Another crucial aspect for applications is the degree of current asymmetry, conveniently measured by the dimensionless diode efficiency $\eta(\hat{n}) = |J_c(\hat{n}) - J_c(-\hat{n})|/[J_c(\hat{n}) + J_c(-\hat{n})]$. A large efficiency, as close to 1 as possible, is desirable for the system to operate as a superconducting diode without having to fine-tune the current magnitude.

In this Letter, we propose and demonstrate theoretically an enhancement mechanism for the SDE efficiency η, specifically for systems with spontaneously broken TRS. While it is clear by symmetry that the condensation of a time-reversal-odd order parameter can affect the critical supercurrent and induce a SDE, we here demonstrate that the supercurrent also couples back to the underlying symmetry-breaking order parameter. If superconductivity and the TRS-breaking order have similar energy scales, this "backaction" can be quite large and, as we demonstrate, can enhance η significantly. Although this mechanism is more generally valid and should apply to different models and forms of the time-reversal-odd order parameter, we use a model inspired by graphene moiré systems; this is motivated by Ref. [25] where a junction-free sample of twisted trilayer graphene was studied and a zero-field SDE with a particularly large η was observed, and by Ref. [34], where it was shown that valley imbalance is the most natural normal-state instability inducing the SDE at zero field. Our work, thus, both provides a possible route to explaining the large η of Ref. [25] and paves the way for the design of zero-field superconducting diodes with large current asymmetries.

Model for SDE.—As motivated above, we study an electronic Hamiltonian of the form

$$\mathcal{H}_c = \sum_{\boldsymbol{k},\nu} \xi_{\boldsymbol{k},\nu} c^\dagger_{\boldsymbol{k},\nu} c_{\boldsymbol{k},\nu} + \Phi_V \sum_{\boldsymbol{k},\nu} \nu c^\dagger_{\boldsymbol{k},\nu} c_{\boldsymbol{k},\nu} + \sum_{\boldsymbol{k},\boldsymbol{q}} \left[\Delta_{\boldsymbol{q}} c^\dagger_{\boldsymbol{k}+\boldsymbol{q}/2,+} c^\dagger_{-\boldsymbol{k}+\boldsymbol{q}/2,-} + \text{H.c.}\right], \quad (1)$$

where $c^\dagger_{\boldsymbol{k},\nu}$ creates an electron in valley $\nu = \pm$ and at momentum $\boldsymbol{k}$. The three terms in $\mathcal{H}_c$ capture the noninteracting band structure of the nearly flat bands at the chemical potential, which obey $\xi_{\boldsymbol{k},\nu} = \xi_{-\boldsymbol{k},-\nu} \equiv \xi_{\boldsymbol{k}\cdot\nu}$ due to TRS, the coupling of the TRS-breaking normal state order (in our case, valley imbalance Φ_V) and of the superconducting order parameter to the electrons, respectively. We suppressed the spin index in Eq. (1) and in the following, but emphasize that our results apply both for spin polarized bands [60,61] and in the spinful case.

To stabilize superconductivity, we take an attractive ($g_c > 0$) interaction $\mathcal{H}_{g_c} = -(g_c/2)\sum_{\boldsymbol{q},\nu,\nu'} C^\dagger_{\boldsymbol{q};\nu,\nu'} C_{\boldsymbol{q};\nu,\nu'}$ with $C_{\boldsymbol{q};\nu,\nu'} = \sum_{\boldsymbol{k}} c_{\boldsymbol{k}+\boldsymbol{q}/2,\nu} c_{-\boldsymbol{k}+\boldsymbol{q}/2,\nu'}$ and perform a decoupling in the intervalley pairing channel, $\langle C_{\boldsymbol{q};\nu,\nu'}\rangle = \nu\delta_{\nu,-\nu'}\Delta_{\boldsymbol{q}}/g_c$; we focus on intervalley pairing because it is favored by TRS for a finite range of Φ_V [34]. For valley polarization, we use $\mathcal{H}_{g_v} = -g_v \sum_{\boldsymbol{k},\boldsymbol{k}',\nu,\nu'} \nu\nu' c^\dagger_{\boldsymbol{k},\nu} c_{\boldsymbol{k},\nu} c^\dagger_{\boldsymbol{k}',\nu'} c_{\boldsymbol{k}',\nu'}$, and the resulting mean-field Hamiltonian reads as $\mathcal{H}_S = \mathcal{H}_c + \sum_{\boldsymbol{q}} |\Delta_{\boldsymbol{q}}|^2/g_c + \Phi_V^2/g_v$. While we will compute the supercurrent systematically below, we start for illustration purposes with a semiphenomenological approach. Integrating out the electrons in $\mathcal{H}_S$ and expanding up to quartic order in $\Delta_{\boldsymbol{q}}$, the change $\delta\mathcal{F}_S := \mathcal{F}[\Delta_{\boldsymbol{q}}, \Phi_V] - \mathcal{F}[0, \Phi_V]$ of the free energy with superconductivity reads as

$$\delta\mathcal{F}_S \sim \sum_{\boldsymbol{q}} a^S_{\boldsymbol{q}} |\Delta_{\boldsymbol{q}}|^2 + b^S \sum_{\boldsymbol{q}_i} \Delta^*_{\boldsymbol{q}_1} \Delta^*_{\boldsymbol{q}_2} \Delta_{\boldsymbol{q}_3} \Delta_{\boldsymbol{q}_4} \delta_{\boldsymbol{q}_1+\boldsymbol{q}_2,\boldsymbol{q}_3+\boldsymbol{q}_4},$$

where we neglected the momentum dependence of the quartic term. It holds $a^S_{\boldsymbol{q}} = 1/g_c - \Gamma_{\boldsymbol{q}}$ with [34]

$$\Gamma_{\boldsymbol{q}} = \frac{1}{2N}\sum_{\boldsymbol{k}} \frac{\tanh\frac{E_{\boldsymbol{k},\boldsymbol{q},+}}{2T} + \tanh\frac{E_{\boldsymbol{k},\boldsymbol{q},-}}{2T}}{E_{\boldsymbol{k},\boldsymbol{q},+} + E_{\boldsymbol{k},\boldsymbol{q},-}}, \tag{2}$$

where N is the number of unit cells and $E_{\boldsymbol{k},\boldsymbol{q},\nu} = \xi_{\boldsymbol{k}+\nu\boldsymbol{q}/2} + \nu\Phi_V$ encodes the normal-state dispersion, associated with the first line of Eq. (1).

The equilibrium superconducting state at given Φ_V is found by minimizing $\delta\mathcal{F}_S$. Restricting the analysis to single-$\boldsymbol{q}$ states, $\Delta_{\boldsymbol{q}} \propto \delta_{\boldsymbol{q},\boldsymbol{q}_0}$, the value of $\boldsymbol{q}_0$ is determined by the minimum of $a^S_{\boldsymbol{q}}$ (the maximum of $\Gamma_{\boldsymbol{q}}$). As expected, the current $\boldsymbol{J}(\boldsymbol{q}) = 2e\Delta_{\boldsymbol{q}}\boldsymbol{v}_{\boldsymbol{q}}$, $\boldsymbol{v}_{\boldsymbol{q}} = \boldsymbol{\nabla}_{\boldsymbol{q}} a^S_{\boldsymbol{q}}$ [30,31,34] vanishes in equilibrium, $\boldsymbol{J}(\boldsymbol{q}_0) = 0$; a supercurrent-carrying state, therefore, corresponds to pairing with $\boldsymbol{q} \neq \boldsymbol{q}_0$. We define the critical current $J_c(\hat{n})$ along $\hat{n}$ as the maximal magnitude of $\boldsymbol{J}(\boldsymbol{q})$ oriented along $\hat{n}$. Therefore, we allowed for finite $\boldsymbol{q}$ in Eq. (1) not only to capture the potential finite-momentum pairing ($\boldsymbol{q}_0 \neq 0$) for sufficiently large Φ_V [14,34], but also to compute the critical current by imposing a certain $\boldsymbol{q} \neq \boldsymbol{q}_0$.

For $\Phi_V = 0$, it holds that $E_{\boldsymbol{k},\boldsymbol{q},\nu} = E_{\boldsymbol{k},-\boldsymbol{q},-\nu}$ and thus $\Gamma_{\boldsymbol{q}} = \Gamma_{-\boldsymbol{q}}$ in Eq. (2). This, in turn, immediately implies $\boldsymbol{J}(\boldsymbol{q}) = -\boldsymbol{J}(-\boldsymbol{q})$ and $J_c(\hat{n}) = J_c(-\hat{n})$, i.e., there is no SDE. This was expected as a consequence of TRS or twofold rotational symmetry, C_{2z}, for that matter—both have to be broken to get $J_c(\hat{n}) \neq J_c(-\hat{n})$. This is achieved by $\Phi_V \neq 0$ [34], leading to a finite SDE efficiency, $\eta = \max_{\hat{n}}\{[|J_c(\hat{n}) - J_c(-\hat{n})|]/[J_c(\hat{n}) + J_c(-\hat{n})]\} \in [0, 1]$. Although generically nonzero by symmetry, it does not guarantee that η can reach high values corresponding to large current asymmetries, $J_c(\hat{n}) \gg J_c(-\hat{n})$—a property desirable for applications of the SDE and relevant fundamentally to understand recent experiments [25].

Phenomenological coupling.—The main result of this work is that η can be significantly enhanced by taking into account that the strength of the valley polarization is affected by the supercurrent or, put differently, Φ_V entering $E_{\boldsymbol{k},\boldsymbol{q},\nu}$ in Eq. (2) also depends on the center of mass momentum $\boldsymbol{q}$ of the Cooper pairs, $\Phi_V \to \Phi_V(\boldsymbol{q})$. Postponing a systematic microscopic computation that treats $\Delta_{\boldsymbol{q}}$ and $\Phi_V(\boldsymbol{q})$ on equal footing, we start with a simpler phenomenological analysis. In this simplified description, we determine $\Phi_V(\boldsymbol{q})$ by minimizing the free energy

$$\mathcal{F}_V \sim a_\Phi \Phi_V^2 + b_\Phi \Phi_V^4 + \Phi_V \sum_{\boldsymbol{q}} |\Delta_{\boldsymbol{q}}|^2 [F(\boldsymbol{q}) + \alpha'' \Phi_V] \tag{3}$$

with respect to Φ_V, where terms involving fifth and higher powers of the order parameters Φ_V, $\Delta_{\boldsymbol{q}}$ are neglected. The first two terms in $\mathcal{F}_V$ determine the value of Φ_V in the absence of superconductivity. Meanwhile, the remaining terms in Eq. (3) capture the key coupling between the momentum of the Cooper pairs and Φ_V. For the last term, we have $\alpha'' > 0$, which can be shown by integrating out the electrons in Eq. (1), and captures that increasing (decreasing) the superconducting order parameter suppresses (enhances) Φ_V. The other term with $F(\boldsymbol{q}) = -F(-\boldsymbol{q})$ describes the fact that superconductivity at finite $\boldsymbol{q}$ breaks TRS and C_{2z} and can, hence, couple to the first power of Φ_V. Motivated by twisted graphene systems, which exhibit C_{3z} rotational symmetry, we write

$$F(\boldsymbol{q}) = \alpha \hat{\boldsymbol{e}}_\epsilon \cdot \boldsymbol{X}(\boldsymbol{q}) + \alpha' \chi(\boldsymbol{q}), \tag{4}$$

where $\boldsymbol{X}(\boldsymbol{q})$ and $\chi(\boldsymbol{q})$ are real valued, periodic on the Brillouin zone, and odd in $\boldsymbol{q}$, and transform as a vector and scalar under C_{3z}, respectively. We use the leading lattice harmonics for $\boldsymbol{X}(\boldsymbol{q})$ and $\chi(\boldsymbol{q})$ (see the Supplemental Material [62] for their explicit form), which, in the limit of small $\boldsymbol{q}$, obey $\boldsymbol{X} \sim (q_x, q_y)^T$ and $\chi(\boldsymbol{q}) \sim q_x(q_x^2 - 3q_y^2)$. Importantly, the first term in Eq. (4) requires finite strain or nematic order which breaks C_{3z} symmetry explicitly. These phenomena, which seem to be ubiquitous in graphene moiré systems [63–69], define a preferred in-plane direction, captured by the unit vector $\hat{\boldsymbol{e}}_\epsilon$. For instance, in the case of strain, $\hat{\boldsymbol{e}}_\epsilon \propto (\epsilon_{xx} - \epsilon_{yy}, \epsilon_{xy} + \epsilon_{yz})^T$, where ϵ_{ij} are the strain-tensor elements. We note that the coupling would also be present if Φ_V was replaced by another order

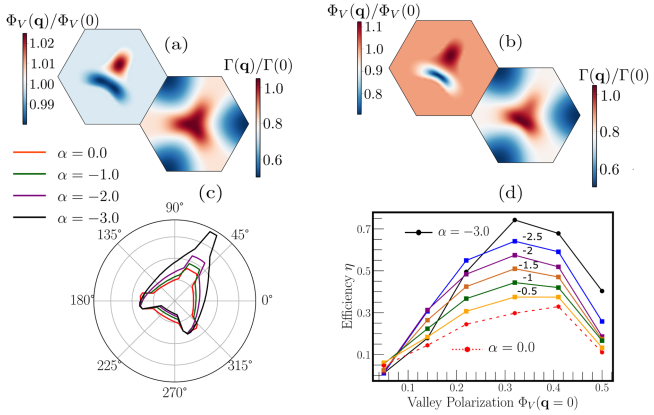

FIG. 1. Phenomenological theory with leading nematic coupling, $\alpha \neq 0$, $\alpha' = \alpha'' = 0$ in Eq. (3). $\Phi_v(\boldsymbol{q})$ and $\Gamma(\boldsymbol{q})$ for (a) $\alpha = -0.5$ and (b) $\alpha = -3.0$ are shown in upper and lower panels, respectively. (c) Angular ($\hat{n}$) dependence of J_c for different α, taking $|\Phi(\boldsymbol{q}=0)| = 0.32$. (d) SDE efficiency η for different α as a function of valley polarization at $\boldsymbol{q} = 0$. We use $g_c^{-1} = 0.8\Gamma_{\boldsymbol{q}=0}[\Phi_V(\boldsymbol{q}=0)]$, $\mu = -0.68$, $\phi = -0.7\pi$, $T = 0.2$, $\hat{\boldsymbol{e}}_\epsilon = (\cos\pi/3, \sin\pi/3)$.

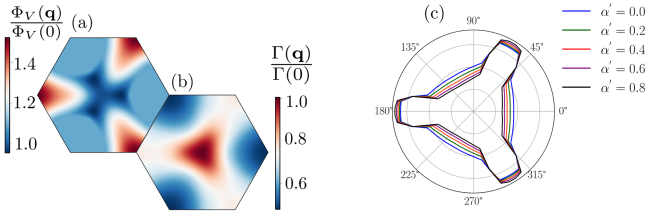

FIG. 2. Phenomenological theory with C_{3z}-symmetric coupling, $\alpha' \neq 0$, $\alpha = 0$, $\alpha'' = 1.0$ in Eq. (3). $\Phi_v(\boldsymbol{q})$ and $\Gamma(\boldsymbol{q})$ in (a) and (b) are shown for $\alpha' = 0.8$, and (c) displays the angular ($\hat{n}$) dependence of J_c for different α'. We use $g_c^{-1} = 0.7\Gamma_{\boldsymbol{q}=0}[\Phi_V = 0.32]$, $\mu = -0.68$, $\phi = -0.7\pi$, $T = 0.2$.

parameter that itself already breaks both TRS and C_{3z} simultaneously [69,70]. The second term in Eq. (4) is finite regardless of whether C_{3z} is broken.

To study the SDE, we self-consistently minimize $\mathcal{F}_V[\Phi_V, \Delta_{\boldsymbol{q}}]$ and $\delta\mathcal{F}_S[\Phi_V, \Delta_{\boldsymbol{q}}]$ with respect to Φ_V and $\Delta_{\boldsymbol{q}}$, respectively, and compute $\boldsymbol{J}(\boldsymbol{q})$, for a *given* $\boldsymbol{q}$ that we impose and that differs from the true equilibrium $\boldsymbol{q}_0$. For concreteness, we use a nearest-neighbor dispersion with finite flux ϕ on the triangular lattice, $\xi_{\boldsymbol{k}} = -\sum_{j=1}^{3} t_j \cos(\boldsymbol{a}_j \cdot \boldsymbol{k} - \phi/3)$ where $\boldsymbol{a}_j$ are three C_{3z}-related primitive vectors. We choose $t_1 = t$, $t_2 = t_3 = t(1+\beta)$ to parametrize the impact of strain ($\propto \beta$) on the dispersion and, for notational simplicity, measure all energies in units of t in the following.

Back action and SDE.—We start with the first term in Eq. (4), i.e., set $\alpha' = \alpha'' = 0$ in $\mathcal{F}_V$. As can be seen in Fig. 1(a), finite α now induces a $\boldsymbol{q}$ dependence in Φ_V, which breaks C_{3z} symmetry as a result of the preferred direction associated with $\hat{\boldsymbol{e}}_\epsilon$. As we set $\beta = 0$ for now, $\Gamma_{\boldsymbol{q}}$ looks virtually C_{3z} symmetric, while larger α will lead to a noticeable asymmetry in $\Gamma_{\boldsymbol{q}}$ as well; see Fig. 1(b). This results from a "backaction mechanism," where a finite supercurrent, which is associated with detuning the center of mass momentum $\boldsymbol{q}_0 \to \boldsymbol{q} + \delta\boldsymbol{q}_0$ of the Cooper pairs away from their equilibrium value $\boldsymbol{q}_0$, changes the strength of Φ_V; as increasing (decreasing) Φ_V will weaken (strengthen) superconductivity, this, in turn, influences $\Gamma_{\boldsymbol{q}}$. This can be thought of as the supercurrent analog of the coupling between the dissipative current and valley polarization observed in graphene moiré systems [71–73]. We note in passing that a sufficiently strong supercurrent can also flip the sign Φ_V in our theory.

This backaction also affects the $\boldsymbol{q}$ dependence of the supercurrent, which allows one to enhance the SDE as can be seen in Fig. 1(c). We further present in Fig. 1(d) the diode efficiency η as a function of $\Phi_V(\boldsymbol{q}=0)$ for different strengths of the backaction. Without backaction ($\alpha = 0$, red dashed line), η does not exceed 30%, corresponding to $J_c(\hat{n}) \simeq 1.86 J_c(-\hat{n})$. In contrast, increasing α and, thus, boosting the backaction mechanism can significantly enhance the SDE, even reaching efficiencies as high as 75% (solid black line), i.e., $J_c(\hat{n}) \simeq 7 J_c(-\hat{n})$.

This enhancement mechanism of the SDE is also possible in the presence of C_{3z}, where $\alpha = 0$, if we take into account finite α' in Eq. (4); see Fig. 2. We can clearly see the induced $\boldsymbol{q}$ (and thus supercurrent) dependence of Φ_V in Fig. 2(a). However, the backaction onto $\Gamma_{\boldsymbol{q}}$ is less clearly seen in Fig. 2(b) at a single α', since it is C_{3z} symmetric with and without it. Most importantly, though, Fig. 2(c) reveals that the subleading backaction ($\alpha = 0$) also enhances the current asymmetry.

Self-consistent theory.—We next turn our attention to a systematic self-consistent formalism. We switch to an action formalism and redefine $c_{\boldsymbol{k},\nu}$ in Eq. (1) as Grassmann variables depending on imaginary time τ. We start from the effective action

$$\mathcal{S} = \int \mathrm{d}\tau \left[\sum_{\boldsymbol{k},\nu} c^\dagger_{\boldsymbol{k},\nu} \partial_\tau c_{\boldsymbol{k},\nu} + \mathcal{H}_c + \mathcal{S}_\Delta + \mathcal{S}_\Phi \right], \quad (5)$$

that captures the desired phenomenology in a minimal setting. In Eq. (5), $\mathcal{S}_\Delta = \sum_{\boldsymbol{q}} [(1/g_c)|\Delta_{\boldsymbol{q}}|^2 + u_\Delta |\Delta_{\boldsymbol{q}}|^4]$ and $\mathcal{S}_\Phi = (1/g_v)\Phi_V^2 + v_{\Phi_V}\Phi_V^4$ are the bare actions of the Hubbard-Stratonovich fields associated with superconductivity and valley polarization, respectively. We include terms up to quartic order (which, e.g., arise after having integrated out electronic degrees of freedom at higher energies) to stabilize coexistence of these two orders, as is seen in experiment [25,34,74].

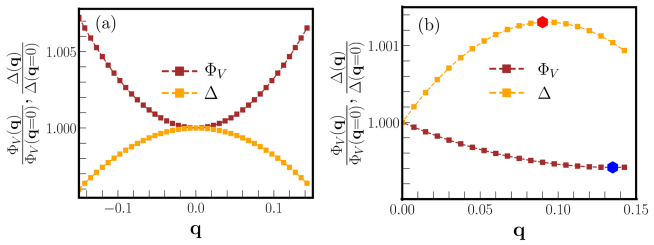

FIG. 3. Coupling of supercurrent to valley polarization within microscopic theory. $\Phi_V(\boldsymbol{q})$ and $\Delta(\boldsymbol{q})$ along one-dimensional momentum cut with angle $\pi/6$ relative to the q_x axis (a) without form factors ($f_{\boldsymbol{k}} = 1$) and (b) with form factors, $f_{\boldsymbol{k}} = \sum_{j=1}^{3} \sin \boldsymbol{a}_j \cdot \boldsymbol{k}$. The red (blue) hexagon denotes the maximum (minimum) of $\Delta(\boldsymbol{q})$ and $\Phi_V(\boldsymbol{q})$, respectively. We use $\beta = 0.6$, $\mu = -1.36$, $g_c = 5.6$, $g_v = 11$, $u_\Delta = 0.25$, $v_\Phi = 0.125$, $T = 0.4$.

The saddle point equations for Φ_V and $\Delta_{\boldsymbol{q}}$ read as

$$\frac{\Phi_V}{g_v} + 2v_\Phi \Phi_V^3 = \frac{1}{4} \sum_{\boldsymbol{k},p=\pm} p \tanh \frac{\mathcal{E}_{\boldsymbol{k},\boldsymbol{q},p}}{2T}, \tag{6a}$$

$$\frac{1}{g_c} + 2u_\Delta |\Delta_{\boldsymbol{q}}|^2 = \sum_{\boldsymbol{k}} \frac{\left(\tanh \frac{\mathcal{E}_{\boldsymbol{k},\boldsymbol{q},+}}{2T} + \tanh \frac{\mathcal{E}_{\boldsymbol{k},\boldsymbol{q},-}}{2T}\right)}{2(\mathcal{E}_{\boldsymbol{k},\boldsymbol{q},+} + \mathcal{E}_{\boldsymbol{k},\boldsymbol{q},-})}, \tag{6b}$$

or $\Delta_{\boldsymbol{q}} = 0$, where $\mathcal{E}_{\boldsymbol{k},\boldsymbol{q},p} = \sqrt{\zeta^2_{\boldsymbol{k},\boldsymbol{q},+} + |\Delta_{\boldsymbol{q}}|^2} + p\zeta_{\boldsymbol{k},\boldsymbol{q},-}$ with $\zeta_{\boldsymbol{k},\boldsymbol{q},\pm} = (E_{\boldsymbol{k},\boldsymbol{q},+} \pm E_{\boldsymbol{k},\boldsymbol{q},-})/2$. As required, Eq. (6b) becomes equivalent to $a^{\mathrm{S}}_{\boldsymbol{q}} = 0$ when expanded to leading order in $\Delta_{\boldsymbol{q}}$.

We solve Eq. (6) self-consistently for both $\Delta_{\boldsymbol{q}}$ and Φ_V for given $\boldsymbol{q}$. This captures the mutual influence of these two orders, as $\Delta_{\boldsymbol{q}}$ and Φ_V enter each other's saddle point equation, Eqs. (6a) and (6b), respectively, via the dispersion $\mathcal{E}$. Broken C_{3z} symmetry is entirely encoded in the parameter β entering the bare normal-state dispersion $\xi_{\boldsymbol{k}}$. Generically, the two coupled saddle point equations are expected to capture any symmetry-allowed coupling term between $\Delta_{\boldsymbol{q}}$ and Φ_V in an effective free-energy expansion, including those in Eq. (3). It turns out, though, that for the simple coupling in $\mathcal{H}_c$, where valley polarization only enters as an imbalance of the chemical potential in the two valleys, we find $\alpha = 0$ in Eq. (4) for any β. This is readily shown by expanding Eq. (6a) in terms of $\delta\Phi_V(\boldsymbol{q}) = \Phi_V(\boldsymbol{q}) - \Phi_V(0)$ at fixed $\Delta(\boldsymbol{q})$ and studying whether Δ and Φ_V are stationary at the same momentum ($\alpha = 0$) or not ($\alpha \neq 0$); see the Supplemental Material [62]. The obtained $\alpha = 0$ implies that the backaction is dominated by the term $\alpha''|\Delta_{\boldsymbol{q}}|^2\Phi_V^2$ in Eq. (4) for small $\boldsymbol{q}$ as can be seen in Fig. 3(a), where $\delta\Phi_V(\boldsymbol{q}) \propto \delta\Delta(\boldsymbol{q}) \sim \boldsymbol{q}^2$ for small $\boldsymbol{q}$. We have checked that generalizing the coupling to $\Phi_V \sum_{\boldsymbol{k},\nu} \nu f_{\boldsymbol{k}\cdot\nu} c^\dagger_{\boldsymbol{k},\nu} c_{\boldsymbol{k},\nu}$, with C_{3z}-invariant form factors $f_{\boldsymbol{k}}$, leads to finite α; this is clearly visible in Fig. 3(b), where

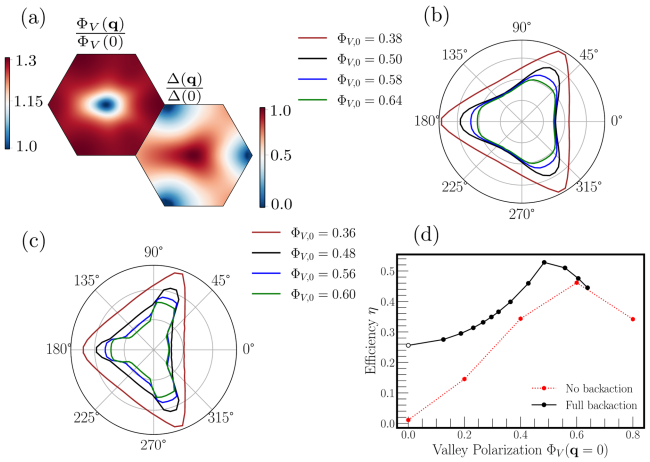

FIG. 4. SDE within self-consistent theory, Eq. (5). (a) $\Phi_V(\boldsymbol{q})$ and $\Delta(\boldsymbol{q})$ in the upper and lower panel, for $|\Phi_V(\boldsymbol{q} = 0)| = 0.48$ and $\beta = 0.6$. Resulting angular dependence of J_c is shown without strain in (b) and with strain ($\beta = 0.6$) in (c). (d) Efficiency η as a function of $\Phi_V(\boldsymbol{q} = 0)$ in presence of strain with backaction (black solid line) and without backaction (red dotted line). The parameters for g_c, T, μ, v_Φ, u_Δ are the same as in Fig. 3; only g_v is varied to change $\Phi_V(\boldsymbol{q} = 0)$.

$\Phi_V(\boldsymbol{q})$ is found to have a finite slope at the maximum (red hexagon) of $\Delta(\boldsymbol{q})$.

SDE in self-consistent theory.—To demonstrate that the enhancement mechanism for the SDE based on the backaction is a robust phenomenon, we here discuss it for the original case without form factors, $f_{\boldsymbol{k}} = 1$, where the leading coupling ($\propto \alpha$) in the phenomenological theory in Eq. (3) is absent. In Fig. 4(a), we plot $\Phi_V(\boldsymbol{q})$ and $\Delta(\boldsymbol{q})$, obtained by solving Eq. (6). We can clearly see the supercurrent-induced change of Φ_V, which is manifestly not C_{3z} invariant, due to $\beta \neq 0$, and exhibits the strongest asymmetry under $\boldsymbol{q} \to -\boldsymbol{q}$ for $\boldsymbol{q}$ along q_x. Owing to the additional coupling terms beyond those in Eq. (3), $\Phi_V(\boldsymbol{q})$ looks different at large $\boldsymbol{q}$ from that shown in Fig. 2(a). However, for our purpose the more important $\Delta(\boldsymbol{q})$ looks very similar to $\Gamma_{\boldsymbol{q}}$ in Fig. 2(b). Evaluating the thermal expectation value of the current operator within the full theory (see the Supplemental Material [62]) as a function of $\boldsymbol{q}$, we compute the directional dependence of the critical current, shown in Figs. 4(b) and 4(c) for $\beta = 0$ and $\beta \neq 0$, respectively. Exactly as in the phenonemological theory, we find that broken C_{3z} symmetry can enhance the SDE and that the current asymmetry first increases with small Φ_V (as significant TRS breaking is needed to generate a large current asymmetry) but then eventually decreases with large Φ_V (as it destabilizes superconductivity and also weakens the backaction). This is also visible in Fig. 4(d), where we plot the SDE efficiency η of the full self-consistent theory (black line) as a function of valley polarization at $\boldsymbol{q} = 0$ and compare it with the situation without backaction (red dashed line); for the latter, we just fix Φ_V at the indicated value $\Phi_V(\boldsymbol{q} = 0)$, independent of $\boldsymbol{q}$

and solve for superconductivity via Eq. (2). We observe that the backaction not only enhances, as before, the maximum value of η that can be achieved, but also increases the efficiency significantly at smaller values of valley polarization. The reason for this amplification is the aforementioned dominance of the α''-like couplings in the self-consistent theory, which enhance $\Phi_V(\boldsymbol{q})$ when suppressing $\Delta_{\boldsymbol{q}}$ with finite $\boldsymbol{q}$; see also Fig. 3(a). So even if we have very small $\Phi_V(\boldsymbol{q}=0)$, valley polarization can reach sizable values at nonzero $\boldsymbol{q}$ due to the coupling to the supercurrent, which in turn enhances the diode effect. This is why η reaches finite values in the limit $\Phi_V(\boldsymbol{q}=0)\to 0^+$ with backaction, while it has to vanish linearly with $\Phi_V(\boldsymbol{q}=0)$ without it in Fig. 4(d). It shows that the proposed backaction mechanism also enhances the *typical* η which can reach large values without the need of fine-tuning $\Phi_V(\boldsymbol{q}=0)$ to its optimal strength.

Conclusion.—We have shown, using both a simple free-energy expansion and a self-consistent theory, that the supercurrent can couple to and, hence, affect the valley polarization Φ_V, which in turn can enhance the SDE efficiency significantly; see Figs. 1(d) and 4(d). Motivated by Ref. [25], this was formulated for a theory applicable to graphene-based systems; however, we expect that the basic mechanism based on coupling of the supercurrent to a TRS-breaking order parameter is more generally valid for zero-field superconducting diodes.

S. B. and M. S. S. acknowledge funding by the European Union (ERC-2021-STG, Project No. 101040651—SuperCorr). M. S. thanks J. I. A. Li and H. Scammell for insightful discussions and comments on the manuscript. S. B. is grateful for discussions with J. A. Sobral, A. Rastogi, B. Putzer, and P. Wilhelm.

Views and opinions expressed are however those of the authors only and do not necessarily reflect those of the European Union or the European Research Council Executive Agency. Neither the European Union nor the granting authority can be held responsible for them.

[1] P. R. Broussard and T. H. Geballe, Critical currents in sputtered Nb-Ta multilayers, Phys. Rev. B **37**, 68 (1988).
[2] X. Jiang, P. J. Connolly, S. J. Hagen, and C. J. Lobb, Asymmetric current-voltage characteristics in type-II superconductors, Phys. Rev. B **49**, 9244 (1994).
[3] A. Papon, K. Senapati, and Z. H. Barber, Asymmetric critical current of niobium microbridges with ferromagnetic stripe, Appl. Phys. Lett. **93**, 172507 (2008).
[4] F. Ando, Y. Miyasaka, T. Li, J. Ishizuka, T. Arakawa, Y. Shiota, T. Moriyama, Y. Yanase, and T. Ono, Observation of superconducting diode effect, Nature (London) **584**, 373 (2020).
[5] Y.-Y. Lyu, J. Jiang, Y.-L. Wang, Z.-L. Xiao, S. Dong, Q.-H. Chen, M. V. Milošević, H. Wang, R. Divan, J. E. Pearson, P. Wu, F. M. Peeters, and W.-K. Kwok, Superconducting diode effect via conformal-mapped nanoholes, Nat. Commun. **12**, 2703 (2021).
[6] W.-S. Du, W. Chen, Y. Zhou, T. Zhou, G. Liu, Z. Zhang, Z. Miao, H. Jia, S. Liu, Y. Zhao, Z. Zhang, T. Chen, N. Wang, W. Huang, Z.-B. Tan, J.-J. Chen, and D.-P. Yu, Superconducting diode effect and large magnetochiral anisotropy in T_d-$MoTe_2$ thin film, arXiv:2303.09052.
[7] A. Sundaresh, J. I. Vayrynen, Y. Lyanda-Geller, and L. P. Rokhinson, Diamagnetic mechanism of critical current nonreciprocity in multilayered superconductors, Nat. Commun. **14**, 1628 (2023).
[8] R. Kealhofer, H. Jeong, A. Rashidi, L. Balents, and S. Stemmer, Anomalous superconducting diode effect in a polar superconductor, Phys. Rev. B **107**, L100504 (2023).
[9] Y. Hou, F. Nichele, H. Chi, A. Lodesani, Y. Wu, M. F. Ritter, D. Z. Haxell, M. Davydova, S. Ilić, O. Glezakou-Elbert, A. Varambally, F. S. Bergeret, A. Kamra, L. Fu, P. A. Lee, and J. S. Moodera, Ubiquitous superconducting diode effect in superconductor thin films, Phys. Rev. Lett. **131**, 027001 (2023).
[10] P. B. Chen, B. C. Ye, J. H. Wang, L. Zhou, X. Lei, Z. Z. Tang, J. N. Wang, J. W. Mei, and H. T. He, Superconducting diode effect in inversion symmetry breaking $MoTe_2$ Josephson junctions, arXiv:2303.07701.
[11] M. Gupta, G. V. Graziano, M. Pendharkar, J. T. Dong, C. P. Dempsey, C. Palmstrøm, and V. S. Pribiag, Gate-tunable superconducting diode effect in a three-terminal Josephson device, Nat. Commun. **14**, 3078 (2023).
[12] C. Baumgartner, L. Fuchs, A. Costa, S. Reinhardt, S. Gronin, G. C. Gardner, T. Lindemann, M. J. Manfra, P. E. Faria Junior, D. Kochan, J. Fabian, N. Paradiso, and C. Strunk, Supercurrent rectification and magnetochiral effects in symmetric Josephson junctions, Nat. Nanotechnol. **17**, 39 (2022).
[13] A. Banerjee, M. Geier, M. A. Rahman, C. Thomas, T. Wang, M. J. Manfra, K. Flensberg, and C. M. Marcus, Phase asymmetry of Andreev spectra from Cooper-pair momentum, Phys. Rev. Lett. **131**, 196301 (2023).
[14] B. Pal, A. Chakraborty, P. K. Sivakumar, M. Davydova, A. K. Gopi, A. K. Pandeya, J. A. Krieger, Y. Zhang, M. Date, S. Ju, N. Yuan, N. B. M. Schröter, L. Fu, and S. S. P. Parkin, Josephson diode effect from Cooper pair momentum in a topological semimetal, Nat. Phys. **18**, 1228 (2022).
[15] J.-K. Kim, K.-R. Jeon, P. K. Sivakumar, J. Jeon, C. Koerner, G. Woltersdorf, and S. S. P. Parkin, Intrinsic supercurrent non-reciprocity coupled to the crystal structure of a van der Waals Josephson barrier, arXiv:2303.13049.
[16] B. Turini, S. Salimian, M. Carrega, A. Iorio, E. Strambini, F. Giazotto, V. Zannier, L. Sorba, and S. Heun, Josephson diode effect in high-mobility INSB nanoflags, Nano Lett. **22**, 8502 (2022).
[17] L. Bauriedl, C. Bäuml, L. Fuchs, C. Baumgartner, N. Paulik, J. M. Bauer, K.-Q. Lin, J. M. Lupton, T. Taniguchi, K. Watanabe, C. Strunk, and N. Paradiso, Supercurrent diode effect and magnetochiral anisotropy in few-layer $NbSe_2$, Nat. Commun. **13**, 4266 (2022).
[18] H. Wu, Y. Wang, Y. Xu, P. K. Sivakumar, C. Pasco, U. Filippozzi, S. S. P. Parkin, Y.-J. Zeng, T. McQueen, and M. N. Ali, The field-free Josephson diode in a van der Waals heterostructure, Nature (London) **604**, 653 (2022).

[19] J. Diez-Merida, A. Diez-Carlon, S. Y. Yang, Y.-M. Xie, X.-J. Gao, K. Watanabe, T. Taniguchi, X. Lu, K. T. Law, and D. K. Efetov, Magnetic Josephson junctions and superconducting diodes in magic angle twisted bilayer graphene, arXiv:2110.01067.

[20] T. Golod and V. M. Krasnov, Demonstration of a superconducting diode-with-memory, operational at zero magnetic field with switchable nonreciprocity, Nat. Commun. **13**, 3658 (2022).

[21] J. Chiles, E. G. Arnault, C.-C. Chen, T. F. Q. Larson, L. Zhao, K. Watanabe, T. Taniguchi, F. Amet, and G. Finkelstein, Non-reciprocal supercurrents in a field-free graphene Josephson triode, Nano Lett. **23**, 5257 (2023).

[22] F. Zhang, M. T. Ahari, A. S. Rashid, G. J. de Coster, T. Taniguchi, K. Watanabe, M. J. Gilbert, N. Samarth, and M. Kayyalha, Reconfigurable magnetic-field-free superconducting diode effect in multi-terminal Josephson junctions, arXiv:2301.05081.

[23] J. Shin, S. Son, J. Yun, G. Park, K. Zhang, Y. J. Shin, J.-G. Park, and D. Kim, Magnetic proximity-induced superconducting diode effect and infinite magnetoresistance in van der Waals heterostructure, Phys. Rev. Res. **5**, L022064 (2023).

[24] K.-R. Jeon, J.-K. Kim, J. Yoon, J.-C. Jeon, H. Han, A. Cottet, T. Kontos, and S. S. P. Parkin, Zero-field polarity-reversible Josephson supercurrent diodes enabled by a proximity-magnetized Pt barrier, Nat. Mater. **21**, 1008 (2022).

[25] J.-X. Lin, P. Siriviboon, H. D. Scammell, S. Liu, D. Rhodes, K. Watanabe, T. Taniguchi, J. Hone, M. S. Scheurer, and J. I. A. Li, Zero-field superconducting diode effect in small-twist-angle trilayer graphene, Nat. Phys. **18**, 1221 (2022).

[26] M. S. Anwar, T. Nakamura, R. Ishiguro, S. Arif, J. W. A. Robinson, S. Yonezawa, M. Sigrist, and Y. Maeno, Spontaneous superconducting diode effect in non-magnetic $Nb/Ru/Sr_2RuO_4$ topological junctions, Commun. Phys. **6**, 290 (2023).

[27] H. Narita, J. Ishizuka, R. Kawarazaki, D. Kan, Y. Shiota, T. Moriyama, Y. Shimakawa, A. V. Ognev, A. S. Samardak, Y. Yanase, and T. Ono, Field-free superconducting diode effect in noncentrosymmetric superconductor/ferromagnet multilayers, Nat. Nanotechnol. **17**, 823 (2022).

[28] A. Gutfreund, H. Matsuki, V. Plastovets, A. Noah, L. Gorzawski, N. Fridman, G. Yang, A. Buzdin, O. Millo, J. W. A. Robinson, and Y. Anahory, Direct observation of a superconducting vortex diode, Nat. Commun. **14**, 1630 (2023).

[29] A. Daido and Y. Yanase, Superconducting diode effect and nonreciprocal transition lines, Phys. Rev. B **106**, 205206 (2022).

[30] A. Daido, Y. Ikeda, and Y. Yanase, Intrinsic superconducting diode effect, Phys. Rev. Lett. **128**, 037001 (2022).

[31] N. F. Q. Yuan and L. Fu, Supercurrent diode effect and finite-momentum superconductors, Proc. Natl. Acad. Sci. U.S.A. **119**, e2119548119 (2022).

[32] J. J. He, Y. Tanaka, and N. Nagaosa, A phenomenological theory of superconductor diodes, New J. Phys. **24**, 053014 (2022).

[33] S. Ilić and F. S. Bergeret, Theory of the supercurrent diode effect in Rashba superconductors with arbitrary disorder, Phys. Rev. Lett. **128**, 177001 (2022).

[34] H. D. Scammell, J. I. A. Li, and M. S. Scheurer, Theory of zero-field superconducting diode effect in twisted trilayer graphene, 2D Mater. **9**, 025027 (2022).

[35] B. Zinkl, K. Hamamoto, and M. Sigrist, Symmetry conditions for the superconducting diode effect in chiral superconductors, Phys. Rev. Res. **4**, 033167 (2022).

[36] Y. Zhang, Y. Gu, P. Li, J. Hu, and K. Jiang, General theory of Josephson diodes, Phys. Rev. X **12**, 041013 (2022).

[37] J. J. He, Y. Tanaka, and N. Nagaosa, The supercurrent diode effect and nonreciprocal paraconductivity due to the chiral structure of nanotubes, Nat. Commun. **14**, 3330 (2023).

[38] B. Zhai, B. Li, Y. Wen, F. Wu, and J. He, Prediction of ferroelectric superconductors with reversible superconducting diode effect, Phys. Rev. B **106**, L140505 (2022).

[39] J. Jiang, M. V. Milošević, Y.-L. Wang, Z.-L. Xiao, F. M. Peeters, and Q.-H. Chen, Field-free superconducting diode in a magnetically nanostructured superconductor, Phys. Rev. Appl. **18**, 034064 (2022).

[40] T. H. Kokkeler, A. A. Golubov, and F. S. Bergeret, Field-free anomalous junction and superconducting diode effect in spin-split superconductor/topological insulator junctions, Phys. Rev. B **106**, 214504 (2022).

[41] M. Chazono, S. Kanasugi, T. Kitamura, and Y. Yanase, Piezoelectric effect and diode effect in anapole and monopole superconductors, Phys. Rev. B **107**, 214512 (2023).

[42] D. Y. Vodolazov and F. M. Peeters, Superconducting rectifier based on the asymmetric surface barrier effect, Phys. Rev. B **72**, 172508 (2005).

[43] T. de Picoli, Z. Blood, Y. Lyanda-Geller, and J. I. Väyrynen, Superconducting diode effect in quasi-one-dimensional systems, Phys. Rev. B **107**, 224518 (2023).

[44] D. Kochan, A. Costa, I. Zhumagulov, and I. Žutić, Phenomenological theory of the supercurrent diode effect: The Lifshitz invariant, arXiv:2303.11975.

[45] Y. Ikeda, A. Daido, and Y. Yanase, Intrinsic superconducting diode effect in disordered systems, arXiv:2212.09211.

[46] Y. Tanaka, B. Lu, and N. Nagaosa, Theory of giant diode effect in d -wave superconductor junctions on the surface of a topological insulator, Phys. Rev. B **106**, 214524 (2022).

[47] D. Wang, Q.-H. Wang, and C. Wu, Symmetry constraints on direct-current Josephson diodes, arXiv:2209.12646.

[48] R. Haenel and O. Can, Superconducting diode from flux biased Josephson junction arrays, arXiv:2212.02657.

[49] H. F. Legg, K. Laubscher, D. Loss, and J. Klinovaja, Parity protected superconducting diode effect in topological Josephson junctions, Phys. Lett. B **108**, 214520 (2023).

[50] J. J. Cuozzo, W. Pan, J. Shabani, and E. Rossi, Microwave-tunable diode effect in asymmetric SQUIDs with topological Josephson junctions, arXiv:2303.16931.

[51] R. S. Souto, M. Leijnse, and C. Schrade, Josephson diode effect in supercurrent interferometers, Phys. Rev. Lett. **129**, 267702 (2022).

[52] Q. Cheng and Q.-F. Sun, Josephson diode based on conventional superconductors and a chiral quantum dot, Phys. Rev. B **107**, 184511 (2023).

[53] J. F. Steiner, L. Melischek, M. Trahms, K. J. Franke, and F. von Oppen, Diode effects in current-biased Josephson junctions, Phys. Rev. Lett. **130**, 177002 (2023).
[54] A. Costa, J. Fabian, and D. Kochan, Microscopic study of the Josephson supercurrent diode effect in 2DEG-based Josephson junctions, Phys. Rev. B **108**, 054522 (2023).
[55] Y.-J. Wei, H.-L. Liu, J. Wang, and J.-F. Liu, Supercurrent rectification effect in graphene-based Josephson junctions, Phys. Rev. B **106**, 165419 (2022).
[56] H. F. Legg, D. Loss, and J. Klinovaja, Superconducting diode effect due to magnetochiral anisotropy in topological insulators and Rashba nanowires, Phys. Rev. B **106**, 104501 (2022).
[57] T. Karabassov, I. V. Bobkova, A. A. Golubov, and A. S. Vasenko, Hybrid helical state and superconducting diode effect in superconductor/ferromagnet/topological insulator heterostructures, Phys. Rev. B **106**, 224509 (2022).
[58] J.-X. Hu, Z.-T. Sun, Y.-M. Xie, and K. T. Law, Josephson diode effect induced by valley polarization in twisted bilayer graphene, Phys. Rev. Lett. **130**, 266003 (2023).
[59] Y.-M. Wu, Z. Wu, and H. Yao, Pair-density-wave and chiral superconductivity in twisted bilayer transition metal dichalcogenides, Phys. Rev. Lett. **130**, 126001 (2023).
[60] E. Morissette, J.-X. Lin, D. Sun, L. Zhang, S. Liu, D. Rhodes, K. Watanabe, T. Taniguchi, J. Hone, J. Pollanen, M. S. Scheurer, M. Lilly, A. Mounce, and J. I. A. Li, Electron spin resonance and collective excitations in magic-angle twisted bilayer graphene, Nat. Phys **19**, 1156 (2023).
[61] U. Zondiner, A. Rozen, D. Rodan-Legrain, Y. Cao, R. Queiroz, T. Taniguchi, K. Watanabe, Y. Oreg, F. von Oppen, A. Stern, E. Berg, P. Jarillo-Herrero, and S. Ilani, Cascade of phase transitions and Dirac revivals in magic-angle graphene, Nature (London) **582**, 203 (2020).
[62] See Supplemental Material at http://link.aps.org/supplemental/10.1103/PhysRevLett.132.046003 for more details and results.
[63] Y. Jiang, X. Lai, K. Watanabe, T. Taniguchi, K. Haule, J. Mao, and E. Y. Andrei, Charge order and broken rotational symmetry in magic-angle twisted bilayer graphene, Nature (London) **573**, 91 (2019).
[64] A. Kerelsky, L. J. McGilly, D. M. Kennes, L. Xian, M. Yankowitz, S. Chen, K. Watanabe, T. Taniguchi, J. Hone, C. Dean, A. Rubio, and A. N. Pasupathy, Maximized electron interactions at the magic angle in twisted bilayer graphene, Nature (London) **572**, 95 (2019).
[65] Y. Cao, D. Rodan-Legrain, J. M. Park, N. F. Q. Yuan, K. Watanabe, T. Taniguchi, R. M. Fernandes, L. Fu, and P. Jarillo-Herrero, Nematicity and competing orders in superconducting magic-angle graphene, Science **372**, 264 (2021).
[66] C. Rubio-Verdú, S. Turkel, Y. Song, L. Klebl, R. Samajdar, M. S. Scheurer, J. W. F. Venderbos, K. Watanabe, T. Taniguchi, H. Ochoa, L. Xian, D. M. Kennes, R. M. Fernandes, Á. Rubio, and A. N. Pasupathy, Moiré nematic phase in twisted double bilayer graphene, Nat. Phys. **18**, 196 (2022).
[67] R. Samajdar, M. S. Scheurer, S. Turkel, C. Rubio-Verdú, A. N. Pasupathy, J. W. F. Venderbos, and R. M. Fernandes, Electric-field-tunable electronic nematic order in twisted double-bilayer graphene, 2D Mater. **8**, 034005 (2021).
[68] J. A. Sobral, S. Obernauer, S. Turkel, A. N. Pasupathy, and M. S. Scheurer, Machine learning microscopic form of nematic order in twisted double-bilayer graphene, Nat. Commun. **14**, 5012 (2023).
[69] N. J. Zhang, Y. Wang, K. Watanabe, T. Taniguchi, O. Vafek, and J. I. A. Li, Electronic anisotropy in magic-angle twisted trilayer graphene, arXiv:2211.01352.
[70] J.-X. Lin, Y. Wang, N. J. Zhang, K. Watanabe, T. Taniguchi, L. Fu, and J. I. A. Li, Spontaneous momentum polarization and diodicity in Bernal bilayer graphene, arXiv:2302.04261.
[71] M. Serlin, C. L. Tschirhart, H. Polshyn, Y. Zhang, J. Zhu, K. Watanabe, T. Taniguchi, L. Balents, and A. F. Young, Intrinsic quantized anomalous Hall effect in a moiré heterostructure, Science **367**, 900 (2020).
[72] A. L. Sharpe, E. J. Fox, A. W. Barnard, J. Finney, K. Watanabe, T. Taniguchi, M. A. Kastner, and D. Goldhaber-Gordon, Emergent ferromagnetism near three-quarters filling in twisted bilayer graphene, Science **365**, 605 (2019).
[73] X. Ying, M. Ye, and L. Balents, Current switching of valley polarization in twisted bilayer graphene, Phys. Rev. B **103**, 115436 (2021).
[74] N. J. Zhang, J.-X. Lin, Y. Wang, K. Watanabe, T. Taniguchi, L. Fu, and J. I. A. Li, Valley ferromagnetism and superconductivity in magic-angle trilayer graphene, arXiv:2209.12964.